applied sciences

MDPI

Review

Impact of LGE-MRI in Arrhythmia Ablation

Paz Garre [1,2], Sara Vázquez-Calvo [1,2], Elisenda Ferro [3,4], Till Althoff [1,2] and Ivo Roca-Luque [1,2,5,*]

1 Institut Clinic Cardiovascular, Hospital Clínic, Universitat de Barcelona, 08036 Barcelona, Spain
2 Institut d'Investigacions Biomèdiques August Pi i Sunyer (IDIBAPS), 08036 Barcelona, Spain
3 Medtronic Iberica, 08970 Sant Joan Despí, Spain
4 Fundació Clínic per a la Recerca Biomèdica (FCRB), 08036 Barcelona, Spain
5 Centro de Investigación Biomédica en Red de Enfermedades Cardiovasculares (CIBERCV), 28029 Madrid, Spain
* Correspondence: iroca@clinic.cat

Abstract: The use of late gadolinium enhancement magnetic resonance imaging (LGE-MRI) in arrhythmia ablation is increasing due to the capacity to detect, quantify and characterize cardiac fibrosis both in atrium and ventricle. Catheter ablation has become a standard treatment for arrhythmias, and LGE-MRI has demonstrated to be a useful tool to plan and guide ablation. Furthermore, recent studies have proved the usefulness in substrate analysis and postablation evaluation. This review will analyze the application and the current role of LGE-MRI to improve strategies for the two main cardiac arrhythmias: Atrial fibrillation and ventricular tachycardia.

Keywords: cardiac magnetic resonance; late gadolinium enhancement; atrial fibrillation; ventricular tachycardia; ablation; fibrosis; electroanatomical mapping

1. Introduction

Magnetic resonance imaging (MRI) has become a cornerstone of the diagnostic and prognostic evaluation of patients with cardiac arrhythmias. It is widely used for qualitative and quantitative evaluation of cardiac conditions and support diagnosis, monitoring disease progression and treatment planning [1]. Nowadays, late gadolinium enhancement (LGE) MRI is being used to detect and quantify cardiac fibrosis in both ventricular and atrial arrhythmias [2–6].

Atrial fibrillation (AF) is the most prevalent sustained cardiac arrhythmia, being observed in up to 2% of the general population and in over 5–10% of the elderly population (>70 years of age). In this sense, due to the ageing of society and demographic changes, the overall prevalence is expected to increase even further [7]. Atrial fibrillation is associated with a fivefold risk of stroke and a threefold incidence of congestive heart failure and doubles the risk of mortality and dementia [8]. Isolation of the pulmonary veins (PV) by catheter ablation has emerged as a first-line therapy for patients with symptomatic AF not responding to pharmaceutical treatment [9]. PVI has achieved high success in paroxysmal atrial fibrillation. Nevertheless, in persistent AF, there is still a high rate of recurrence. A very recent study (ERASE AF) demonstrated that ablation of extra PV areas with low voltage detected with mapping catheters is helpful in these patients. In this sense, MRI could play a role in detecting these areas with LGE.

Ventricular tachycardia (VT) is the most frequent etiology of sudden cardiovascular death (SCD) [10]. In patients with structural heart disease, VT is frequent and catheter ablation has become a standard treatment [11,12], being the main mechanism responsible for a re-entrant circuit [13–15]. In this sense, there is an area of slow conduction of intermediate tissue (so called border zone (BZ)) inside the core scar connecting regions of healthy tissue. These areas of slow conduction are referred to as conducting channels (CCs) which can be rigorously defined during ablation procedures using electroanatomical maps (EAMs) [15–18]. On the other hand, MRI allows the depiction of the BZ, healthy tissue and

check for updates

Citation: Garre, P.; Vázquez-Calvo, S.; Ferro, E.; Althoff, T.; Roca-Luque, I. Impact of LGE-MRI in Arrhythmia Ablation. *Appl. Sci.* **2023**, *13*, 3862. https://doi.org/10.3390/app13063862

Academic Editor: Julio Garcia Flores

Received: 31 January 2023
Revised: 6 March 2023
Accepted: 9 March 2023
Published: 17 March 2023

Copyright: © 2023 by the authors. Licensee MDPI, Basel, Switzerland. This article is an open access article distributed under the terms and conditions of the Creative Commons Attribution (CC BY) license (https://creativecommons.org/licenses/by/4.0/).

core scar, identifying also CCs. A great concordance between EAMs and images obtained by MRI has been reported. Moreover, in a recent study [19] MRI has been carried out post mortem in cases of sudden cardiac death to research cardiac morphological alterations. Despite advancements in ablation technology and better understanding of arrhythmic substrates, VT recurrence rates are still high [20–23]. For this reason, there is a clinical need to improve the characterization of the VT substrate and the efficacy of VT ablation. In this context, LGE-MRI may play an important role.

The objective of this review is to analyse the application of LGE-MRI to improve ablation strategies for the two main cardiac arrhythmias: AF and VT.

2. Use of LGE-MRI for the Detection of Fibrosis

2.1. Principles of LGE

LGE-MRI for the detection of myocardial fibrosis was already described in the late 1990s. Its validation was firstly performed with a canine model with controlled myocardial infarction and LGE-MRI was compared with histology [24]. Contrast agents that use mainly gadolinium are able to diffuse freely into the interstitium but are unable to pass through intact cell membranes, leading to their accumulation in the extracellular space.

Fibrosis replacement produces an expansion of extracellular space so there is an increase in the volume of the distribution of gadolinium. More important, there is a prolonged washout of the gadolinium due the decreased number of capillary vessels in the scar tissue [25,26]. Regarding T1 sequence, gadolinium contrast agents decrease the T1 relaxation time of adjacent tissue. Therefore, LGE enhancement produces an increased signal intensity in T1-weighted MRI images. In addition, other diseases related to the expansion of the extracellular space can be shown by LGE, such as oedema and inflammation formation. Given the lack of specificity for fibrotic tissue detection, the lesion assessment can be challenging [27].

2.2. Protocol of Image Acquisition and LGE Analysis

To date, there is no agreement on the best standardized way to acquire MRI images for the detection of myocardial fibrosis [28–31]. Either 3T or 1.5 scanners can be used to acquire postcontrast images applying fast 3D gradient echo series with fat suppression and ECG gating. Subsequent inversion recovery sequences are used to nullify the signal of healthy myocardium and improve signal intensity and T1 contrast. The optimum inversion time (TI) that suppress healthy tissue (typically 250–300 ms) is initially determined empirically. Scar areas will thus appear hyperenhanced relative to healthy myocardium. Adjustment of TI values during acquisition may be necessary to accommodate incremental T1 values of the normal tissue owing to gadolinium washout. For this reason, ECG gating is important to limit motion artifacts and the MRI acquisition window is limited to less to 20% of the RR interval. For patients with AF, cardioversion is often recommended prior to the study to improve image quality [30,32]. Finally, in some patients another limiting factor could be the need for long breath-holds. To solve that limitation, free-breathing 3D navigators can be used that suppress respiratory artefacts through respiratory gating. Typical LGE-MRI sequences result in a voxel size of 1.25 × 1.25 × 2.5 mm with scan times of 10–15 min, depending on heart rate and breathing patterns.

Regarding myocardial fibrosis, to obtain high-quality LGE-MRI images to evaluate it, the time delay between contrast injection and image acquisition is crucial, as the LGE amount depends on wash-in and washout kinetics. Despite there being no official consensus, usually LGE-MRI acquisition is performed 15–25 min (atrium) or 7–15 min (ventricle) after gadolinium contrast agent injection. The time delay may even be adjusted for each patient due to individual perfusion (cardiovascular function) and washout kinetics (renal function).

In our centre, the acquisition of ventricle images is performed 10–15 min after an intravenous gadolinium injection, and 20 min in the atrium.

2.3. Image Acquisition for Patients with Cardiac Devices

Most patients scheduled for VT ablation are individuals with established cardiomyopathy who carry an implantable cardioverter defibrillator (ICD) implanted for primary or secondary prevention. This issue represents a major limitation for MRI because of security and also because of hyperintense image artefacts that can be caused by the device.

Regarding safety, several studies have shown an extremely low risk of device-related complications in patients who undergo cardiac MRI, not only in MRI conditional devices, but also in the case of theoretical MRI nonconditional devices. With adequate intraprocedural programming of the device, MRI is safe in patients with MRI nonconditional devices [33–35]. In this sense, the main issue with patients with cardiac devices is the quality of MRI images due to the possible artefacts related to the ICD. Artefacts can occur when metallic ICD components distort the magnetic field [36,37] making it difficult to obtain clear images using LGE-MRI. The effect of ICD artefacts are most prominent in the anterior wall, and in patients with left sided devices, in the anterior and apical left ventricle. Some studies have suggested that limited spectral bandwidth of the inversion pulse used in LGE-MRI is the primary cause of device-related artefacts [38,39]. To avoid those artefacts, particular wideband MRI sequences have been recently developed, increasing the bandwidth of the inversion and excitation pulses. Therefore, the use of wideband sequences can minimize device-related artefacts and, subsequently, overcome the image artefact, making LGE-MRI robust for myocardial characterization [33,40,41]. Many centres including ours are now applying these wideband sequences, avoiding device-related artefacts and achieving high quality images, even in areas closed to the ICD. In fact, our group has recently proved a strong correlation between wideband LGE-MRI and electroanatomical maps [42]. In this study [42] the accuracy of wideband sequences to detect CCs previously located in EAMs was analysed for 13 patients with an ICD and a wideband sequence. The accuracy of CCs identified was 85.1% and the positive predicting value was 92.5%.

3. Image Post-Processing (Pre-Procedural)

3.1. Image Processing: Segmentation and Fibrosis Detection

Post-processing is necessary to acquire a 3D anatomical reconstruction of the chamber of interest and to identify, analyse and evaluate the scarring tissue. To acquire this 3D anatomical segmentation, there is a great deal of established open-source and commercial software for image post-processing.

The two steps required to achieve this 3D anatomical structure are segmentation of the anatomical chamber (LA and/or RA and PPVV in the case of AF and LV and/or RV in the case of VT) and detection of fibrotic and scarring areas inside the segmented anatomical structure.

I. Segmentation of anatomical structures

Accurate segmentation is required for scar analysis and fibrosis visualization. The segmentation process was performed manually. Clinicians or engineers segment the atrial wall or the myocardium manually: An accurate slice-by-slice 2D tracing of the LA wall and endocardial and epicardial myocardium to confine the region of interest (ROI) while avoiding anatomical structures (aortic ring, valves, papillary muscles, etc.), the blood pool, fat, etc. Currently, the different segmentation software programs have semiautomatic tools available. Therefore, the manual process may be used after this automatic segmentation to refine the results.

II. Detection of fibrotic tissue

Once the anatomy is properly segmented, the fibrotic regions (LGE) can be assessed qualitatively by visual assessment or quantitatively by using different thresholding techniques. To apply thresholding techniques, different approaches with different algorithms have been improved for the detection of arrhythmogenic areas. To date, there is limited reproducibility across centres because there is no single standardized method for LGE image analysis.

Obtaining a consistent internal reference for normalization and validated signal intensity thresholds that can accurately differentiate between healthy and scar tissue are crucial for quantifying LGE. The reason is that T1-weighted imaging relies on signal intensity contrast instead of directly measured absolute values.

Different methods have been validated for atrial fibrosis quantification (Table 1) [29–31,43–47]. Each method uses distinct internal references and thresholds. As an internal reference, the mean signal intensity of the blood pool is used extensively by numerous groups. Our group has recently validated a method quantifying signal intensity ratios using the mean signal intensity of the left atrial (LA) blood pool as a reference (signal intensity of each given voxel/mean signal intensity of the blood) [29]. The atrium thresholds to characterize healthy myocardium (signal intensity ratio $\leq$ 1.2) and fibrotic tissue (signal intensity ratio > 1.32) were derived from distinct cohorts including both young healthy individuals and post-AF ablation patients. Subsequently these cut-offs were verified in various studies in comparison with voltage mapping during ablation procedures and they were correlated with clinical endpoints [6,48,49] (Figure 1).

Table 1. LGE-MRI post-processing defining thresholds for fibrosis analysis.

	Reference	Model	n	Reference for Normalization	Defined Thresholds
Atrial Fibrosis	Peters et al., 2007 [31]	Human	23	LA blood pool signal intensity	"Minimum threshold which eliminates most left atrial blood pool pixels"
	Oakes et al., 2009 [30]	Human	81	Normal tissue	Mean signal intensity (normal tissue) + (2–4) SD
	Khurram et al., 2014 [47]	Human	75	Mean LA blood pool signal intensity	Fixed IIR threshold: upper limit of normal > 0.97 and dense scar > 1.6
	Harrison et al., 2014 [43]	Animal	16	Mean LA blood pool signal intensity	"2.3 SD for LGE post ablation and 3.3 SD for LGE chronically"
	Dewire et al., 2014 [46]	Human	60	Mean LA blood pool signal intensity	Universal threshold (abnormal myocardium: IIR > 0.97 and <1.61; dense scar: IIR > 1.61)
	Harrison et al., 2015 [44]	Human	20	Mean LA blood pool signal intensity	No universal threshold. Visualization of signal intensities in SD from reference
	Benito el al., 2017 [29]	Human	40	Mean LA blood pool signal intensity	Fixed IIR threshold: upper limit of normal = 1.2 and dense scar > 1.32
	Kurose et al., 2020 [45]	Human	30	Healthy atrial wall	>2 SDs above the mean of healthy left atrium wall
LV Fibrosis	Amado et al., 2004 [50]	Animal	13	Healthy myocardial segment	Mean signal intensity (noninfarcted myocardium region) + (1–6 SD)
	Yan et al., 2006 [51]	Human	144	Healthy myocardial segment	BZ: 2–3 SDs and scar > 3 SDs above remote myocardium
	Andreu et al., 2011 [52]	Human	12	Maximal myocardial signal	Scar > 60% of maximal signal intensity
	Fernandez-Armenta et al., 2013 [53]	Human	21	Maximal myocardial signal	Healthy tissue < 40%, BZ: 40–60% and scar > 60% of maximal signal intensity
	Cochet et al., 2013 [54]	Human	9	Maximal myocardial signal	BZ: 35–50% and scar > 50% of maximal signal intensity

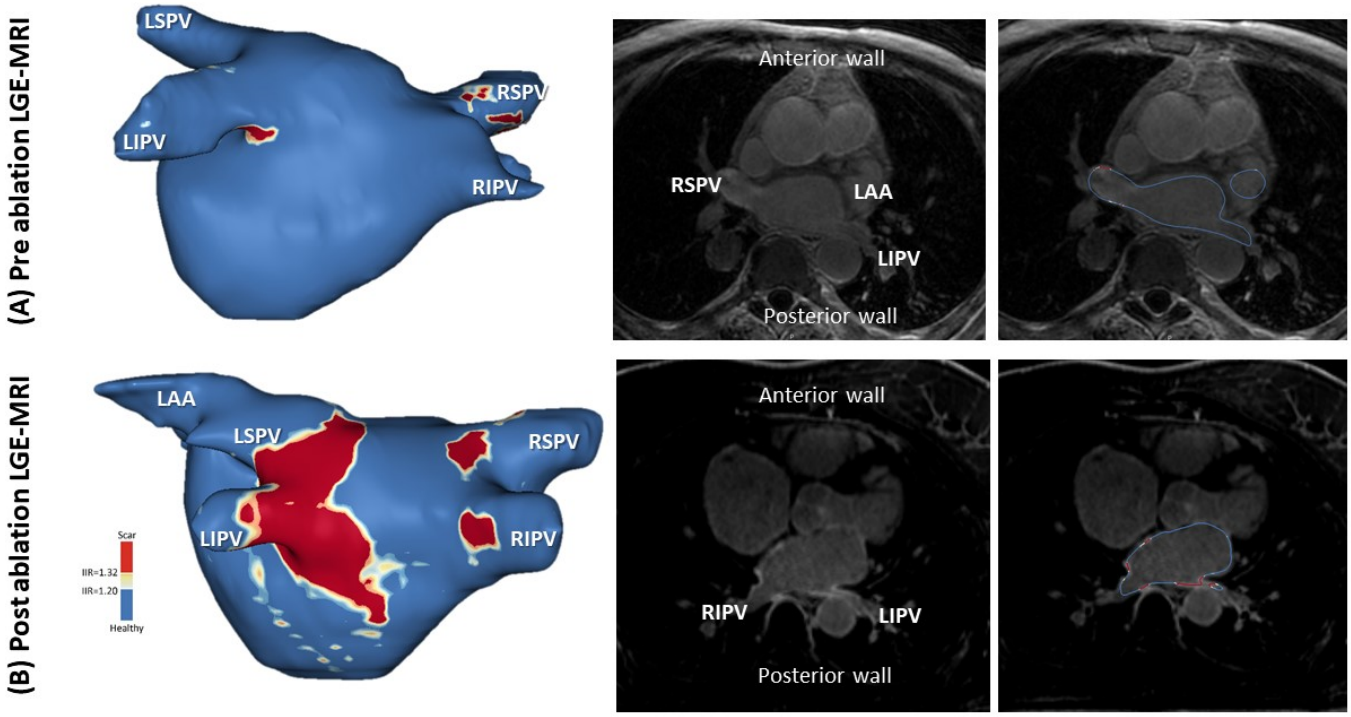

Figure 1. Postero-anterior view of three-dimensional left atrium reconstruction of LGE-MRI. 3D-LGE-LA reconstruction includes colour-coding based on image intensity ratios with thresholds for border zone (yellow 1.2–1.32) and dense scar (red > 1.32). (**A**) First line corresponds to preprocedural LGE-MRI and (**B**) second corresponds to a post-ablation LGE-MRI (3 months after PVI). LAA = left atrial appendage; LIPV = left inferior pulmonary vein; LSPV = left superior pulmonary vein; RIPV = right inferior pulmonary vein; RSPV = right superior pulmonary vein.

The most interesting approaches to detect and quantify fibrosis in LGE-MRI of the left atrial wall are carefully benchmarked by Pontecorboli et al. [2]. This review provides a critical analysis of the different methods to detect and quantify fibrosis in LGE-MRI, stating their advantages and limitations.

Likewise, for ventricular fibrosis quantification, various thresholds and methods have been verified (Table 1) [50–54]. Table 1 summarizes the main studies defining thresholds for LV. The most commonly used approach is the full width at half maximum (FWHM), which is a fixed thresholding method in which a fixed intensity threshold is defined as half of the maximum intensity of a user-selected hyperenhanced region. Another method is to define remote "healthy" myocardial segments as an internal reference for normalization. Another common method is the fixed-model approach, whereby intensities are thresholded to a fixed number of standard deviations (SD) from the mean intensity of the nulled myocardium or blood pool [55]. This is known as the n-SD method.

Our group study found that the correlation with EAM voltage mapping was reached with the thresholds of <40% as healthy tissue and >60% as a dense scar of the maximum signal intensity (Figure 2).

3.2. Deep Learning-Based Methods

With the development of artificial intelligence techniques, the application of deep learning to fibrosis and substrate visualization has also been studied, leading to the development of a fully automated key for LGE-MRI segmentation. An increasing number of various deep learning models using convolutional neural networks (for example, U-Net [56]) have demonstrated encouraging results in the segmentation of cardiac substructures. Goodfellow et al. 2016 [57] mathematically detail these deep neural networks.

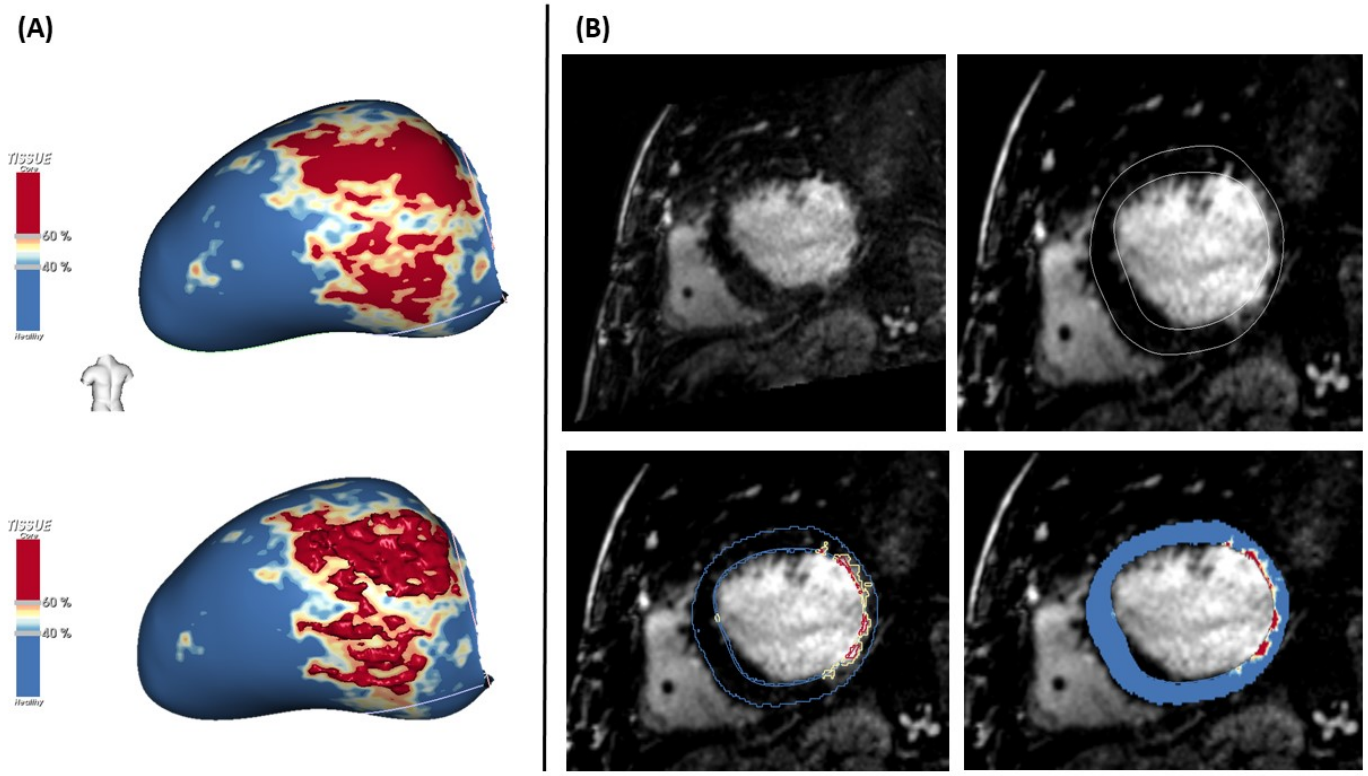

Figure 2. (**A**) Three-dimensional left ventricle reconstruction of LGE-MRI. LGE-based colour-coding is used to differentiate LV dense scar (red > 60% of maximum signal intensity) from border zone (yellow, 40–60% of maximum signal intensity) and healthy tissue (blue < 40%). (**B**) Raw images of LGE-MRI in a patient with chronic MI. Semiautomatic segmentation of epicardium and endocardium with detection of dense scar and border zone is shown.

4. Use of the Processed LGE-MRI for Ablation Procedures

LGE-MRI in VT or AF ablation procedures has proved to be an important tool to plan and guide ablation. Regarding planification, LGE-MRI allows us to perform a preprocedural assessment of cardiac anatomy and myocardial scar (location of conducting channels in the case of VT and PPVV gaps in AF), to decide the optimal access approach (especially in VT where both endocardial and epicardial approaches can be selected) and exclude intracardiac thrombus. In addition, 3D-LGE-MRI reconstruction can be visualized side by side or merged with electroanatomical maps during the procedure. In VT ablation, for example, MRI-aided ablation has demonstrated a lower need for RF delivery, higher noninducibility rates after substrate ablation, and a higher VT recurrence-free survival [58].

4.1. Determination of the Optimal Access Approach

In VT ablation, the location of the myocardial fibrosis is important for determining and designing ablation access: An epicardial approach for patients with epicardial or transmural scars and an endocardial approach for those without epicardial or transmural scars. In addition, LGE-MRI accurately defines intramural scarring, which is a major determinant of VT ablation failure [59]. For this specific case, ablation techniques such as septal alcholization [60], bipolar ablation or ablation using needle ablation catheters can be chosen to enhance outcomes [61].

4.2. Exclusion of Intracardiac Thrombus

In recent years, DE-MRI has been well validated as an accurate technique for the detection of left thrombi [62,63]. It is important in both VT and AF ablation to determine the presence of thrombus because patients with heart failure are at increased risk for thromboembolic events.

4.3. Integration of LGE-MRI and Electroanatomical Map (EAM) during Ablation

Several electroanatomical advanced mapping systems that display bipolar voltage maps and activation maps on a 3D reconstruction of the intracardiac chamber of interest have become available over the past few decades. Each system uses a different technology to generate a 3D image, record electrograms, and localize the electrode catheter in space. Current ablation techniques are heavily reliant on EAM systems (Carto (New York, NY, USA), Biosense Webster, Inc. (Irvine, CA, USA); NAVX (Paris, France), St Jude Medical (Saint Paul, MN, USA); Rhythmia Mapping, Boston Scientific Inc., (Boston, MA, USA).

Electroanatomical systems have been validated for anatomical and electrical accuracy in the atria as well as the ventricles [64–66]. However, there is an important limitation: the 3-dimensional reconstructions from catheters can provide inaccurate data on scar characteristics and could under- or overestimate the extent of scarring and arrhythmogenic substrate. This is due to different reasons: the influence of the electrode size, interelectrode spacing, angle of the incoming wavefront to the mapping catheter [60,67], and contact of the catheter with tissue (especially for those without a contact force sensor). Henceforth, EAMs can hardly be considered the gold standard of substrate definition. Moreover, it must be considered that low voltage detected in the EAM is not always equivalent to fibrosis and vice versa. Fibrosis distribution and fibrosis architecture and the possibility of far-field detection of the healthy tissue in the border of the fibrosis could affect the amplitude of the electrogram detected in the EAM.

Integration of imaging data into EAM systems provides more information about the arrhythmogenic substrate. Therefore, it is possible to merge the EAM with the 3D LGE-MRI reconstruction. Successful integration (with high accuracy) between EAM and MRI has been demonstrated in several studies [53,66,68].

For the merging process, landmarks in both the 3D reconstruction and EAM must be placed (one or more, depending on the system). The selected points to be used as the landmarks or fiducials must be in an identifiable and distinguishable place in the mapped anatomies (for example, the mitroaortic union, LV apex, the ostium of the pulmonary veins, etc.) with a certain angulation that enables them to be placed in the same direction. Once these points are selected, the estimated corresponding location of this endocardial point is marked on the imported 3D MRI surface reconstruction, thus creating a 'landmark pair'. At this point, the navigation system superimposes the 3D MRI surface reconstruction onto the real-time electroanatomic map with different algorithms, depending on each system (visual alignment, surface registration, etc.). Once the integration is completed, the user is able to navigate with the catheters over the 3D MRI reconstruction, visualizing and localizing the scar and the fibrotic tissue.

4.4. LGE-MRI for AF Ablation

The use of LGE-MRI for the assessment of fibrosis in the atrium has not become routine clinical practice. This is because the wall thickness of the atrium is lower than 1 mm, which is near the limit of spatial resolution of MRI, and due to less extensive and more diffuse fibrosis in comparison with the fibrosis in the ventricle. Nevertheless, recent improvements have been developed in MRI acquisition, including 3D navigated inversion recovery sequences to enhance signal-to-noise ratios and resolution, allowing valid atrium characterization [30,69]. These advances are now making LGE-MRI a widely accepted tool for assessing lesions, stratifying risks and selecting appropriate patients for AF ablation in many specialized centres [3].

Many other studies since then have tried to identify LGE-MRI predictors of recurrence after PVI ablation, and the degree of atrial fibrosis was confirmed to be an important predictor. In a retrospective study including patients undergoing AF ablation, there was an observed 45% increased risk of recurrence for each 10% increase in atrial fibrosis at the 5-year follow-up [70]. These data were supported by findings from another cohort of 165 patients. Patients with an amount of LGE less than 35% had favourable ablation outcomes regardless of AF persistence at baseline, whereas those with LGE greater than

35% had a higher rate of AF recurrence in the first year of follow-up after ablation [71]. In the DECAAF multicentre study [72], 260 patients who underwent PVI were included, and the extent of fibrosis in the LA was categorized as 1 (<10% of the atrial wall), 2 (>10% to <20%), 3 (>20% to <30%) and 4 (>30%). Recurrent arrhythmia during follow-up was direct and graded: from 15% in the stage I group to 51% in the stage IV group. In a subsequent randomized study, catheter ablation of left atrial fibrosis was proposed [73]. The benefit of ablation of these areas could not be demonstrated by this study. This result was supported by other randomized trials, where MRI fibrosis ablation plus PVI was not more effective than PVI alone [74].

Another important potential use of LGE-MRI is to guide repeated ablation procedures, as most cases of AF recurrence after PVI ablation are associated with areas of incomplete ablation or gaps around the pulmonary veins [49,75] (Figure 3). Some studies indicate that those gaps can be identified by LGE-MRI with high accuracy [6,48,49,76]. Badger et al. 2010 [75] demonstrated that LGE-MRI is able to confirm a PVI gap with very high predictive values. Bisbal et al. 2014 [6] showed for the first time that the elimination of gaps detected by LGE MRI generates a reisolation of PPVV in the majority of cases. In this particular study, the LGE-MRI reconstruction was merged with the EAM, so the operator was blinded to electrical information, only isolating gaps localized in the MRI. Reisolation was acquired in 95.6% of the reconnected PVs. In addition to guiding redo procedures, gap detection by LGE-MRI has been considered a predictor of AF recurrence. Linhart et al. 2018 [69] found that the relative gap length calculated as the absolute gap length divided by total length of the ablation line measured during MRI at 3 months of follow-up was a marker predicting AF recurrence 1 year after PVI.

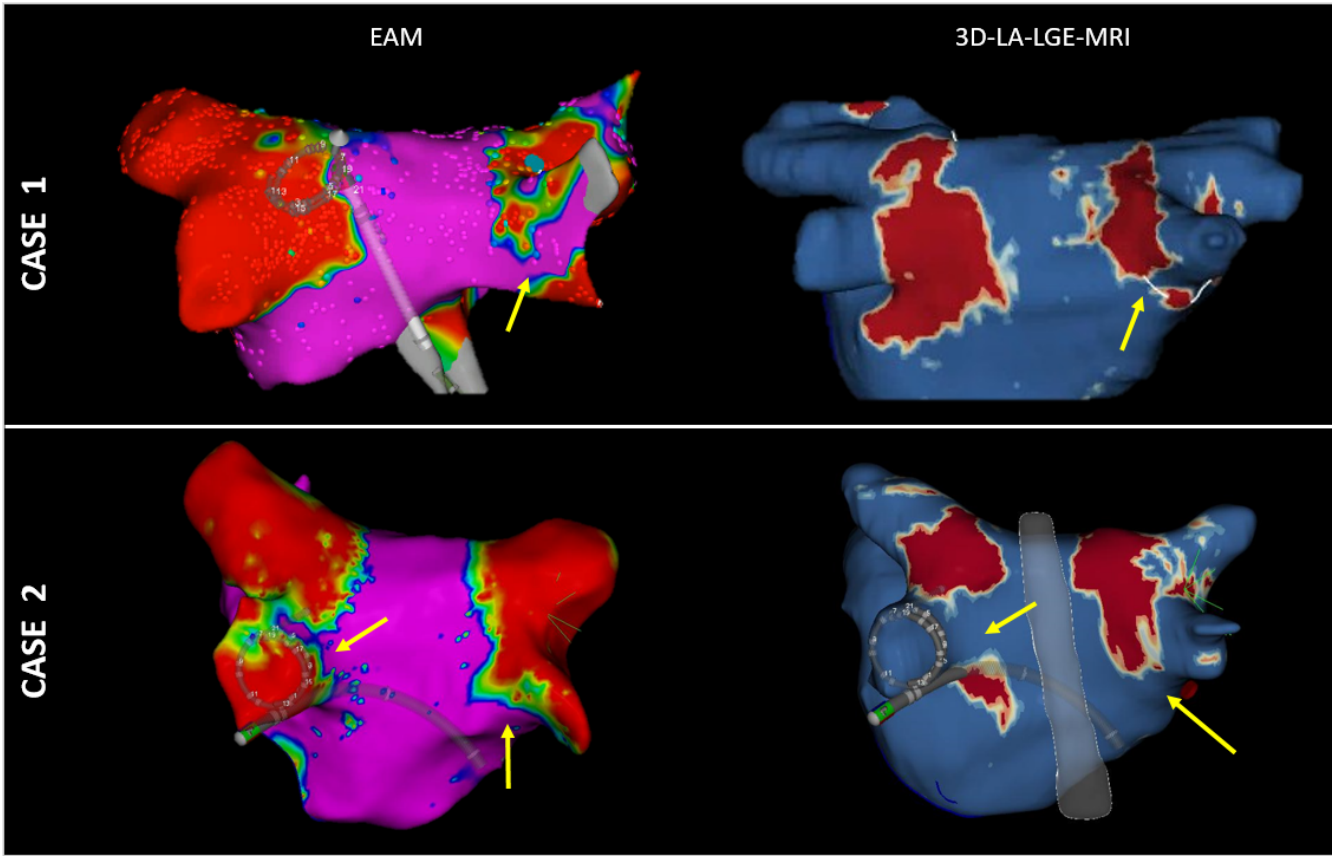

Figure 3. Agreement between EAM voltage map and LGE-MRI gap localisation. From (**left**) to (**right**), voltage map with gaps localised during a repeated ablation intervention. Right, gaps localised at the same region by prior LGE-MRI 3 months post first ablation. Yellow arrows indicate detected EAM gaps and LGE-MRI discontinuities, respectively.

4.5. LGE-MRI for VT Ablation

The use of LGE-MRI in patients undergoing VT ablation is increasing, especially for the preprocedural assessment of the cardiac anatomy and myocardial scarring and for intraprocedural integration.

On the one hand, the use of LGE-MRI provides accurate knowledge of the arrhythmic substrate, including the critical VT isthmuses, the BZ areas and CCs, supporting ablation strategies [52,54,58,77]. The identification of these specific areas has been very useful in cases of ischaemic cardiomyopathy [52,54,58,77]. Moreover, LGE-MRI is also very helpful in cases of nonischaemic cardiomyopathy (NICM). In this sense, some studies have demonstrated that the location of scar in NICM, is also useful for the ablation procedure [78]. This is because the ablation technique and the type of tachycardia is related to the location of scar tissue. Similarly, the effectiveness of using MRI for selecting the appropriate ablation technique was demonstrated in a study involving 80 patients with both NICM and ischemic cardiomyopathy (ICM). In that study, the epicardial or endocardial access was chosen based on MRI. In addition, in case of the intramural substrate, the distance of the scar to the right and left endocardium was used to decided how to approach this substrate [79]. Figure 4 shows an example of the correspondence of LGE-MRI 3D reconstruction with an EAM map.

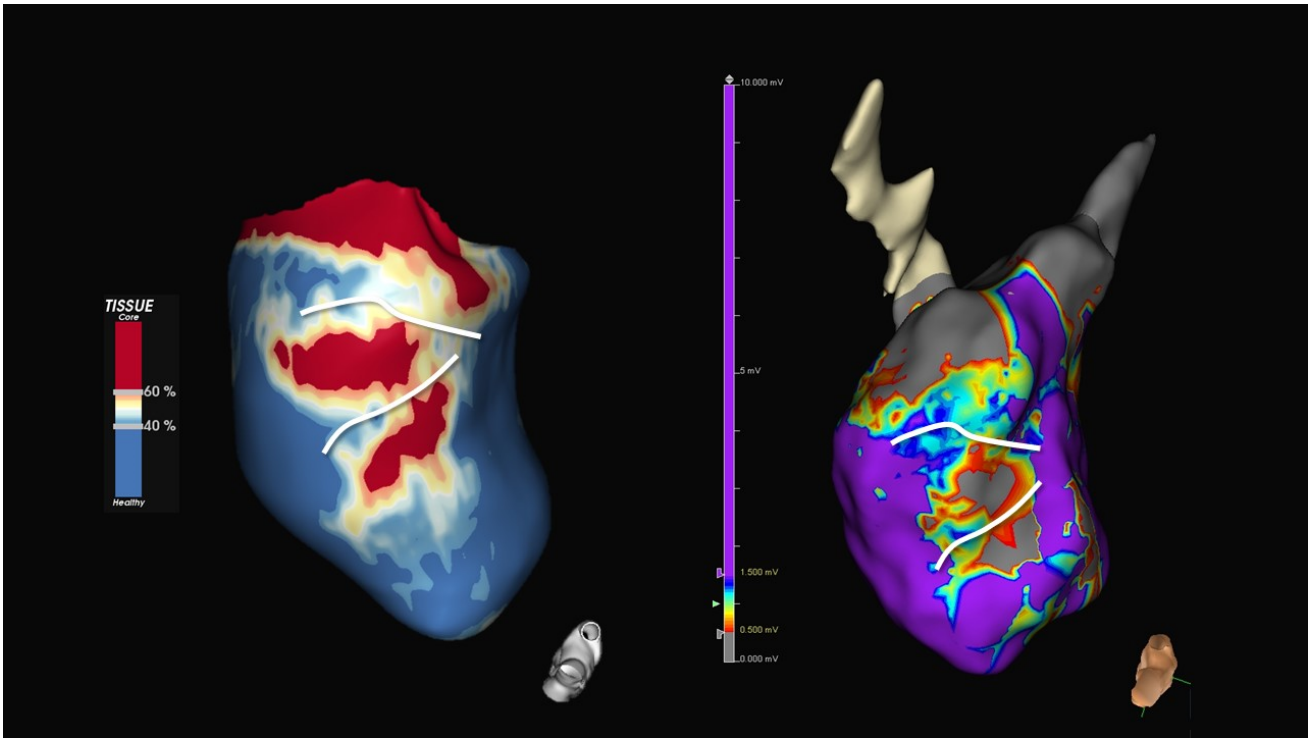

Figure 4. Example of correlation of the 3D-VI reconstruction from LGE-MRI with electroanatomical voltage map. From left to right: LGE-MRI map (colour-coding: blue: healthy tissue, yellow: border zone and red: core scar) with two clear conducting channels (white line); and electroanatomical map high density voltage map showing septal scar (colour-coding: purple: healthy tissue, red: border zone and grey: core scar), with conducting channels at the same region as compared to the LGE-MRI.

On the other hand, in relation to EAMs, studies have not only demonstrated the feasibility of integration during the ablation procedure and a good correlation between 3D-LV reconstruction and EAMs [52,79,80], but have also shown that the scars in MRI scans were larger compared to those detected by EAMs. Moreover, some VT isthmuses were found in regions identified as scar by MRI, but were nonvisible in EAMs [65]. These kinds of studies underscore the value of integrating LGE and EAM for comprehensive scar characterization, particularly in the context of defining infarct BZs, nontransmural scars, and small subepicardial scars [65]. This role of preprocedural MRI to aid procedural access

has also been related to a lower VT recurrence rate, improving the ablation results. A study in patients with ischemic heart disease and epicardial substrate identified prior to ablation by MRI showed that those patients that underwent ablation with epicardial access had better results in terms of VT recurrence, compared to patients who underwent exclusively the endocardial approach [80].

Finally, there is a clear role of MRI in predicting the risk of VT recurrence, even without integration images into the EAM. In a study by Quinto et al. [81], 110 patients who underwent VT ablation with preprocedural LGE-MRI were analysed, identifying MRI-related factors that were clearly linked to a higher rate of VT recurrence, such as mass of border zone and total scar, septal substrate or midmural and transmural CCs. Similarly, in a smaller study [82], scar area was also linked to clinical outcomes, such as VT recurrence. Another study [83] involving 25 non ischemic patients, also verified that the extension of septal LGE was associated with a higher rate of VT recurrence.

5. Conclusions

LGE-MRI constitutes the gold standard for noninvasive characterization of arrhythmogenic myocardial substrate in AF and VT. Its usefulness in both preprocedural planning, substrate analysis and post-ablation evaluation has been proved, even though more technological developments are needed to implement it into routine practice.

6. Limitations

Some limitations need to be addressed. First, consistent methodological and analytical standards defining fibrotic tissue characterization are needed to achieve reproducibility of results between centres. The use of the same values and methods to define fibrotic tissue, will promote the implementation in clinical practice. Second, there is also no homogenous method for integrating MRI-3D into the navigation system. Each group used different structures for merging (pulmonary veins, right ventricle, aortic roof, pulmonary artery, etc.). A more standardized method for using MRI to facilitate ablation would be beneficial for increasing its practical use. In the area of VT ablation, the assessment of ablation lesions has been investigated in small series [28,84,85]. More research is required to confirm and evaluate the usefulness of LGE-MRI in the evaluation of ventricular ablation lesions. Finally, despite new MRI scans, spatial resolution could be insufficient to detect small areas of fibrosis in the atrium wall due to its thickness. In the same line, some types of interstitial fibrosis could be underdetected with conventional LGE, and T1 mapping needs to be improved for clinical practice.

Author Contributions: Conceptualization: P.G., S.V.-C. and E.F., writing: P.G.; review: S.V.-C. and E.F.; and supervision: T.A. and I.R.-L. All authors have read and agreed to the published version of the manuscript.

Funding: This study was supported by Hospital Clinic de Barcelona/Instituto de Salud Carlos III (ISCIII) PI20/00693/CB16/11/00354.

Institutional Review Board Statement: Not applicable.

Informed Consent Statement: Not applicable.

Data Availability Statement: Not applicable.

Conflicts of Interest: I.R.-L. have served as consultants for Boston Scientific and Abbott Medical. T.A. has received research grants for investigator-initiated trials from Biosense Webster.

References

1. Kim, H.W.; Farzaneh-Far, A.; Kim, R.J. Cardiovascular magnetic resonance in patients with myocardial infarction. *J. Am. Coll. Cardiol.* **2009**, *55*, 1–16. [CrossRef] [PubMed]
2. Pontecorboli, G.; Figueras i Ventura, R.M.; Carlosena, A.; Benito, E.; Prat-Gonzales, S.; Padeletti, L.; Mont, L. Use of delayed-enhancement magnetic resonance imaging for fibrosis detection in the atria: A review. *Europace* **2017**, *19*, 180–189. [CrossRef] [PubMed]

3. Hindricks, G.; Potpara, T.; Dagres, N.; Arbelo, E.; Bax, J.J.; Blomstrom-Lundqvist, C.; Boriani, G.; Castella, M.; Dan, G.A.; Dilaveris, P.E.; et al. ESC guidelines for the diagnosis and management of atrial fibrillation developed in collaboration with the European Association of Cardio-Thoracic Surgery (EACTS). *Eur. Heart J.* **2021**, *42*, 373–498. [CrossRef] [PubMed]
4. Cronin, E.M.; Bogun, F.M.; Maury, P.; Peichl, P.; Chen, M.; Namboodiri, N.; Aguinaga, L.; Leite, L.R.; Al-Khatib, S.; Anter, E.; et al. 2019 HRS/EHRA/APHRS/LAHRS expert consensus statement on catheter ablation of ventricular arrhythmias: Executive summary. *Europace* **2020**, *22*, 450–495. [CrossRef]
5. Berruezo, A.; Penela, D.; Jáuregui, B.; Soto-Iglesias, D. The role of imaging in catheter ablation of ventricular arrhythmias. *Pacing Clin. Electrophysiol.* **2021**, *44*, 1115–1125. [CrossRef]
6. Bisbal, F.; Guiu, E.; Cabanas-Grandío, P.; Berruezo, A.; Prat-Gonzalez, S.; Vidal, B.; Garrido, C.; Andreu, D.; Fernandez-Armenta, J.; Tolosana, J.M.; et al. CMR-guided approach to localize and ablate gaps in repeat AF ablation procedure. *JACC Cardiovasc. Imaging* **2014**, *7*, 653–663. [CrossRef]
7. Feinberg, W.M.; Blackshear, J.L.; Laupacis, A.; Kronmal, R.; Hart, R.G. Prevalence, age distribution and gender of patients with atrial fibrillation: Analysis and implications. *Arch. Intern. Med.* **1995**, *155*, 469–473. [CrossRef]
8. January, C.T.; Wann, L.; Alpert, J.S.; Calkins, H.; Cigarroa, J.E.; Cleveland, J.C., Jr.; Conti, J.B.; Ellinor, P.T.; Ezekowitz, M.D.; Field, M.E.; et al. AHA/ACC/HRS guideline for the management of patients with atrial fibrillation: Executive summary: A report of the American College of Cardiology/American Heart Association Task Force on Practice Guidelines and the Heart Rhythm Society. *J. Am. Coll. Cardiol.* **2014**, *64*, 2246–2280. [CrossRef]
9. Calkins, H.; Kuck, K.H.; Cappato, R.; Brugada, J.; Camm, A.J.; Chen, S.A. 2012 HRS/EHRA/ECAS expert consensus statement on catheter and surgical ablation of atrial fibrillation: Recommendations for patient selection, procedural techniques, patient management and follow-up, definitions, endpoints, and research trial design. *Europace* **2012**, *14*, 528–606. [CrossRef]
10. John, R.M.; Tedrow, U.B.; Koplan, B.A.; Albert, C.M.; Epstein, L.M.; Sweeney, M.O.; Miller, A.L.; Michaud, G.; Stevenson, W. Ventricular arrhythmias and sudden cardiac death. *Lancet* **2012**, *380*, 1520–1529. [CrossRef]
11. Tung, R.; Vaseghi, M.; Frankel, D.S.; Vergara, P.; Di Biase, L.; Nagashima, K.; Yu, R.; Vangala, S.; Tseng, C.-H.; Choi, E.-K.; et al. Freedom from recurrent ventricular tachycardia after catheter ablation is associated with improved survival in patients with structural heart disease: An International VT Ablation Center Collaborative Group study. *Heart Rhythm* **2015**, *12*, 1997–2007. [CrossRef]
12. Dukkipati, S.R.; Koruth, J.S.; Chouddry, S.; Miller, M.A.; Whang, W.; Reddy, V.Y. Catheter ablation of ventricular. *J. Am. Coll. Cardiol.* **2017**, *70*, 2924–2941. [CrossRef]
13. De Bakker, J.M.T.; Van Capelle, F.J.L.; Janse, M.J.; Wilde, A.A.M.; Coronel, R.; Becker, A.E.; Dingemans, K.P.; van Hemel, N.M.; Hauer, R.N. Reentry as a cause of ventricular tachycardia in patients with chronic ischemic heart disease: Electrophysiologic and anatomic correlation. *Circulation* **1988**, *77*, 589–606. [CrossRef]
14. Harada, T.; Stevenson, W.G.; Kocovic, D.Z.; Friedman, P.L. Catheter ablation of ventricular tachycardia after myocardial infarction: Relation of endocardial sinus rhythm late potentials to the reentry circuit. *J. Am. Coll. Cardiol.* **1997**, *30*, 1015–1023. [CrossRef]
15. Mountantonakis, S.E.; Park, R.E.; Frankel, D.S.; Hutchinson, M.D.; Dixit, S.; Cooper, J.; Callans, D.; Marchlinski, F.E.; Gerstenfeld, E.P. Relationship between voltage map "channels" and the location of critical isthmus sites in patients with post-infarction cardiomyopathy and ventricular tachycardia. *J. Am. Coll. Cardiol.* **2013**, *61*, 2088–2095. [CrossRef]
16. Bogun, F.; Marine, J.E.; Oral, H.; Pelosi, F.; Morady, F. Relative timing of isolated potentials during post-infarction ventricular tachycardia and sinus rhythm. *J. Interv. Card. Electrophysiol.* **2004**, *10*, 65–72. [CrossRef]
17. Arenal, A.; Glez-Torrecilla, E.; Ortiz, M.; Villacastín, J.; Fdez-Portales, J.; Sousa, E.; del Castillo, S.; de Isla, L.P.; Jimenez, J.; Almendral, J. Ablation of electrograms with an isolated, delayed component as treatment of unmappable monomorphic ventricular tachycardias in patients with structural heart disease. *J. Am. Coll. Cardiol.* **2003**, *41*, 81–92. [CrossRef]
18. Bogun, F.; Good, E.; Reich, S.; Elmouchi, D.; Igic, P.; Lemola, K.; Tschopp, D.; Jongnarangsin, K.; Oral, H.; Chugh, A.; et al. Isolated potentials during sinus rhythm and pace-mapping within scars as guides for ablation of post-infarction ventricular tachycardia. *J. Am. Coll. Cardiol.* **2006**, *47*, 2013–2019. [CrossRef]
19. Bertozzi, G.; Cafarelli, F.P.; Ferrara, M.; Di Fazio, N.; Guglielmi, G.; Cipolloni, L.; Manetti, F.; La Russa, R.; Fineschi, V. Sudden Cardiac Death and Ex-Situ Post-Mortem Cardiac Magnetic Resonance Imaging: A Morphological Study Based on Diagnostic Correlation Methodology. *Diagnostics* **2022**, *12*, 218. [CrossRef]
20. Aziz, Z.; Shatz, D.; Raiman, M.; Upadhyay, G.A.; Beaser, A.D.; Besser, S.A. Targeted ablation of ventricular tachycardia guided by wavefront discontinuities during sinus rhythm: A new functional substrate mapping strategy. *Circulation* **2019**, *140*, 1383–1397. [CrossRef]
21. Willems, S.; Tilz, R.R.; Steven, D.; Kääb, S.; Wegscheider, K.; Gellér, L.; Meyer, C.; Heeger, C.-H.; Metzner, A.; Sinner, M.F.; et al. Preventive or deferred ablation of ventricular tachycardia in patients with ischemic cardiomyopathy and implantable defibrillator (Berlin VT): A multicenter randomized trial. *Circulation* **2020**, *2020*, 1057–1067. [CrossRef] [PubMed]
22. Hadjis, A.; Frontera, A.; Rosario, L.; Bisceglia, C.; Bognoni, L.; Foppoli, L.; Lipartiti, F.; Paglino, G.; Radinovic, A.; Tsitsinakis, G.; et al. Complete electroanatomic imaging of the diastolic pathway is associated with improved. *Circ. Arrhythm. Electrophysiol.* **2020**, *2020*, 927–937. [CrossRef]
23. Quinto, L.; Sanchez-Somonte, P.; Alarcón, F.; Garre, P.; Castillo, À.; San Antonio, R. Ventricular tachycardia burden reduction after substrate ablation: Predictors of recurrence. *Heart Rhythm* **2021**, *18*, 896–904. [CrossRef] [PubMed]

24. Kim, R.J.; Fieno, D.S.; Parrish, T.B.; Harris, K.; Chen, E.-L.; Simonetti, O.; Bundy, J.; Finn, J.P.; Klocke, F.J.; Judd, R.M. Relationship of MRI delayed contrast enhancement to irreversible injury, infarct age, and contractile function. *Circulation* **1999**, *100*, 1992–2002. [CrossRef]
25. Bing, R.; Dweck, M.R. Myocardial fibrosis: Why image, how to image and clinical implications. *Heart* **2019**, *105*, 1832–1840. [CrossRef]
26. Mewton, N.; Liu, C.Y.; Croisille, P. Assessment of myocardial fibrosis with cardiovascular magnetic resonance. *J. Am. Coll. Cardiol.* **2011**, *57*, 891–903. [CrossRef]
27. Kiuchi, K.; Fukuzawa, K.; Nogami, M.; Watanabe, Y.; Takami, M.; Izawa, Y.; Negi, N.; Kyotani, K.; Mori, S.; Hirata, K.-I. Visualization of intensive atrial inflammation and fibrosis after cryoballoon ablation: PET/MRI and LGE-MRI analysis. *J. Arrhythm.* **2021**, *37*, 52–59. [CrossRef]
28. Dickfeld, T.; Kato, R.; Zviman, M.; Lai, S.; Meininger, G.; Lardo, A.C.; Roguin, A.; Blumke, D.; Berger, R.; Calkins, H.; et al. Characterization of radiofrequency ablation lesions with gadolinium-enhanced cardiovascular magnetic resonance imaging. *J. Am. Coll. Cardiol.* **2006**, *47*, 370–378. [CrossRef]
29. Benito, E.M.; Carlosena-Remirez, A.; Guasch, E. Left atrial fibrosis quantification by late gadolinium-enhanced magnetic resonance: A new method to standardize the thresholds for reproducibility. *Europace* **2017**, *19*, 1272–1279. [CrossRef]
30. Oakes, R.S.; Badger, T.J.; Kholmovski, E.G. Detection and quantification of left atrial structural remodeling with delayed-enhancement magnetic resonance imaging in patients with atrial fibrillation. *Circulation* **2009**, *119*, 1758–1767. [CrossRef]
31. Peters, D.C.; Wylie, J.V.; Hauser, T.H.; Kissinger, K.V.; Botnar, R.M.; Essebag, V.; Josephson, M.E.; Manning, W.J. Detection of pulmonary vein and left atrial scar after catheter ablation with three-dimensional navigator-gated delayed enhancement MR imaging: Initial experience. *Radiology* **2007**, *243*, 690–695. [CrossRef]
32. Vijayakumar, S.; Kholmovski, E.; McGann, C.; Marrouche, N.F. Dependence of contrast to noise ratio between ablation scar and other tissues on patient heart rate and flip angle for late gadolinium enhancement imaging of the left atrium. *J. Cardiovasc. Magn. Reson.* **2012**, *14* (Suppl. S1), O107. [CrossRef]
33. Do, D.H.; Eyvazian, V.; Bayoneta, A.J.; Hu, P.; Finn, J.P.; Bradfield, J.S. Cardiac magnetic resonance imaging using wideband sequences in patients with non-conditional cardiac implanted electronic devices. *Heart Rhythm* **2018**, *15*, 218–225. [CrossRef]
34. Seewoster, T.; Lobe, S.; Hilbert, S.; Bollmann, A.; Sommer, P.; Lindemann, F.; Bacevičius, J.; Schöne, K.; Richter, S.; Döring, M.; et al. Cardiovascular magnetic resonance imaging in patients with cardiac implantable electronic devices: Best practice and real-world experience. *Europace* **2019**, *19*, 818–823. [CrossRef]
35. Flett, A.S.; Hasleton, J.; Cook, C.; Hausenloy, D.; Quarta, G.; Ariti, C.; Muthurangu, V.; Moon, J.C. Evaluation of techniques for the quantification of myocardial scar of differing etiology using cardiac magnetic resonance. *JACC Cardiovasc. Imaging* **2011**, *4*, 150–156. [CrossRef]
36. Dickfeld, T.; Tian, J.; Ahmad, G.; Jimenez, A.; Turgeman, A.; Kuk, R.; Peters, M.; Saliaris, A.; Saba, M.; Shorofsky, S.; et al. MRI-guided ventricular tachycardia ablation: Integration of late gadoliniumenhanced 3D scar in patients with implantable cardioverterdefibrillators. *Circ. Arrhythm. Electrophysiol.* **2011**, *4*, 172–184. [CrossRef]
37. Sasaki, T.; Hansford, R.; Zviman, M.M. Quantitative assessment of artifacts on cardiac magnetic resonance imaging of patients with pacemakers and implantable cardioverter-defibrillators. *Circ. Cardiovasc. Imaging* **2011**, *4*, 662–670. [CrossRef]
38. Rashid, S.; Rapacchi, S.; Shivkumar, K.; Plotnik, A.; Finn, J.P.; Hu, P. Modified wideband three-dimensional late gadolinium enhancement MRI for patients with implantable cardiac devices. *Magn. Reson. Med.* **2016**, *75*, 572–584. [CrossRef]
39. Rashid, S.; Rapacchi, S.; Vaseghi, M. Improved late gadolinium enhancement MR imaging for patients with implanted cardiac devices. *Radiology* **2014**, *270*, 269–274. [CrossRef]
40. Bhuva, A.N.; Kellman, P.; Graham, A.; Ramlall, M.; Boubertakh, R.; Feuchter, P.; Hawkins, A.; Lowe, M.; Lambiase, P.D.; Sekhri, N.; et al. Clinical impact of cardiovascular magnetic resonance with optimized myocardial scar detection in patients with cardiac implantable devices. *Int. J. Cardiol.* **2019**, *15*, 72–78. [CrossRef]
41. Hilbert, S.; Weber, A.; Nehrke, K.; Bornert, P.; Schnackenburg, B.; Oebel, S. Artefact-free late gadolinium enhancement imaging in patients with implanted cardiac devices using a modified broadband sequence: Current strategies and results from a real-world patient cohort. *Europace* **2018**, *20*, 801–807. [CrossRef] [PubMed]
42. Roca-Luque, I.; Van Breukelen, A.; Alarcon, F.; Garre, P.; Tolosana, J.M.; Borras, R. Ventricular scar channel entrances identified by new wideband cardiac magnetic resonance sequence to guide ventricular tachycardia ablation in patients with cardiac defibrillators. *Europace* **2020**, *22*, 598–606. [CrossRef] [PubMed]
43. James, L.H.; Henrik, K.J.; Sarah, A.P.; Amedeo, C.; Anne, K.G.; Lars, Ø.B.; Steen, F.; Pedersen, J.F.; Bentzon, C.K.; Rashed, K.; et al. Cardiac magnetic resonance and electroanatomical mapping of acute and chronic atrial ablation injury: A histological validation study. *Eur. Heart J.* **2014**, *35*, 1486–1495. [CrossRef]
44. Harrison, J.L.; Sohns, C.; Linton, N.W.; Karim, R.; Williams, S.E.; Rhode, K.S.; Gill, J.; Cooklin, M.; Rinaldi, C.A.; Wright, M.; et al. Repeat left atrial catheter ablation: Cardiac magnetic resonance prediction of endocardial voltage and gaps in ablation lesion sets. *Circ. Arrhythm. Electrophysiol.* **2015**, *8*, 270–278. [CrossRef] [PubMed]
45. Kurose, J.; Kiuchi, K.; Fukuzawa, K. Lesion characteristics between cryoballoon ablation and radiofrequency ablation with a contact-force sensing catheter: Late-gadolinium enhancement magnetic resonance imaging assessment. *J. Cardiovasc. Electrophysiol.* **2020**, *31*, 2572–2581. [CrossRef]

46. Dewire, J.; Khurram, I.M.; Pashakhanloo, F.; Spragg, D.; Marine, J.E.; Berger, R.D. The association of pre-existing left atrial fibrosis with clinical variables in patients referred for catheter ablation of atrial fibrillation. *Clin. Med. Insights Cardiol.* **2014**, *8* (Suppl. S1), 25–30. [CrossRef]
47. Khurram, I.M.; Beinart, R.; Zipunnikov, V.; Dewire, J.; Yarmohammadi, H.; Sasaki, T.; Spragg, D.D.; Marine, J.E.; Berger, R.D.; Halperin, H.R.; et al. Magnetic resonance image intensity ratio, a normalized measure to enable interpatient comparability of left atrial fibrosis. *Heart Rhythm* **2014**, *11*, 85–92. [CrossRef]
48. Quinto, L.; Cozzari, J.; Benito, E.; Alarcón, F.; Bisbal, F.; Trotta, O.; Caixal, G.; Antonio, R.S.; Garre, P.; Prat-Gonzalez, S.; et al. Magnetic resonance guided re-ablation for atrial fibrillation is associated with a lower recurrence rate: A case-control study. *Europace* **2020**, *22*, 1805–1811. [CrossRef]
49. Fochler, F.; Yamaguchi, T.; Kheirkahan, M. Late gadolinium enhancement magnetic resonance imaging guided treatment of post atrial fibrillation ablation recurrent arrhythmia. *Circ. Arrhythm. Electrophysiol.* **2019**, *12*, e007174. [CrossRef]
50. Amado, L.; Gerber, B.; Gupta, S.; Rettmann, D.; Szarf, G.; Schock, R.; Nasir, K.; Kraitchman, D.; Lima, J. Accurate and objective infarct sizing by contrastenhanced magnetic resonance imaging in a canine myocardial infarction model. *J. Am. Coll. Cardiol.* **2004**, *44*, 2383–2389. [CrossRef]
51. Yan, A.T.; Shayne, A.J.; Brown, K.A.; Gupta, S.N.; Chan, C.W.; Luu, T.M.; Di Carli, M.F.; Reynolds, H.G.; Stevenson, W.G.; Kwong, R.Y. Characterization of the peri-infarct zone by contrast-enhanced cardiac magnetic resonance imaging is a powerful predictor of postmyocardial infarction mortality. *Circulation* **2006**, *114*, 32–39. [CrossRef]
52. Andreu, D.; Berruezo, A.; Ortiz-Pérez, J.T.; Silva, E.; Mont, L.; Borràs, R.; de Caralt, T.M.; Perea, R.J.; Fernández-Armenta, J.; Zeljko, H.; et al. Integration of 3D electroanatomic maps and magnetic resonance scar characterization into the navigation system to guide ventricular tachycardia ablation. *Circ. Arrhythm. Electrophysiol.* **2011**, *4*, 674–683. [CrossRef]
53. Fernandez-Armenta, J.; Berruezo, A.; Andreu, D. Threedimensional architecture of scar and conducting channels based on high resolution ce-CMR: Insights for ventricular tachycardia ablation. *Circ. Arrhythm. Electrophysiol.* **2013**, *6*, 528–537. [CrossRef]
54. Cochet, H.; Komatsu, Y.; Sacher, F. Integration of merged delayed-enhanced magnetic resonance imaging and multidetector computed tomography for the guidance of ventricular tachycardia ablation: A pilot study. *J. Cardiovasc. Electrophysiol.* **2013**, *24*, 419–426. [CrossRef]
55. Roca-Luque, I.; Rivas-Gándara, N.; Francisco-Pascual, J.; Rodriguez-Sanchez, J.; Cuellar-Calabria, H.; Rodriguez-Palomares, J.; García-Del Blanco, B.; Pérez-Rodon, J.; Santos-Ortega, A.; Rosés-Noguer, F.; et al. Preprocedural imaging to guide transcoronary ethanol ablation for refractory septal ventricular tachycardia. *J. Cardiovasc. Electrophysiol.* **2019**, *30*, 448–456. [CrossRef]
56. Ronneberger, O.; Fischer, P.; Brox, T. U-Net: Convolutional networks for biomedical image segmentation. In *Medical Image Computing and Computer-Assisted Intervention—MICCAI 2015*; Lecture Notes in Computer Science; Navab, N., Hornegger, J., Wells, W., Frangi, A., Eds.; Springer: Cham, Switzerland, 2015; Volume 9351, pp. 234–241. [CrossRef]
57. Goodfellow, I.; Bengio, Y.; Courville, A. *Deep Learning*; MIT Press: Cambridge, MA, USA, 2016.
58. Gupta, S.; Desjardins, B.; Baman, T.; Ilg, K.; Good, E.; Crawford, T.; Oral, H.; Pelosi, F.; Chugh, A.; Morady, F.; et al. Delayed-enhanced MR scar imaging and intraprocedural registration into an electroanatomical mapping system in post-infarction patients. *JACC Cardiovasc. Imaging* **2012**, *5*, 207–210. [CrossRef]
59. Bogun, F.M.; Desjardins, B.; Good, E.; Gupta, S.; Crawford, T.; Oral, H.; Ebinger, M.; Pelosi, F.; Chugh, A.; Jongnarangsin, K.; et al. Delayed-enhanced magnetic resonance imaging in nonischemic cardiomyopathy: Utility for identifying the ventricular arrhythmia substrate. *J. Am. Coll. Cardiol.* **2009**, *53*, 1138–1145. [CrossRef]
60. Takigawa, M.; Relan, J.; Martin, R.; Kim, S.; Kitamura, T.; Frontera, A.; Cheniti, G.; Vlachos, K.; Massoullié, G.; Martin, C.A.; et al. Effect of bipolar electrode orientation on local electrogram properties. *Heart Rhythm* **2018**, *15*, 1853–1861. [CrossRef]
61. Kumar, S.; Tedrow, U.B.; Stevenson, W.G. Adjunctive interventional techniques when percutaneous catheter ablation for drug refractory ventricular arrhythmias fail: A contemporary review. *Circ. Arrhythm. Electrophysiol.* **2017**, *10*, e003676. [CrossRef]
62. Weinsaft, J.W.; Kim, H.W.; Shah, D.J.; Klem, I.; Crowley, A.L.; Brosnan, R.; James, O.G.; Patel, M.R.; Heitner, J.; Parker, M.; et al. Detection of left ventricular thrombus by delayed-enhancement cardiovascular magnetic resonance prevalence and markers in patients with systolic dysfunction. *J. Am. Coll. Cardiol.* **2008**, *52*, 148–157. [CrossRef]
63. Weinsaft, J.W.; Kim, R.J.; Ross, M.; Krauser, D.; Manoushagian, S.; LaBounty, T.M.; Cham, M.D.; Min, J.K.; Healy, K.; Wang, Y.; et al. Contrast-enhanced anatomic imaging as compared to contrast enhanced tissue characterization for detection of left ventricular thrombus. *JACC Cardiovasc. Imaging* **2009**, *2*, 969–979. [CrossRef] [PubMed]
64. Stevenson, W.G.; Delacretaz, E.; Friedman, P.L. Identification and ablation of macroreentrant ventricular tachycardia with the CARTO electroanatomical mapping system. *Pacing Clin. Electrophysiol.* **1998**, *21*, 1448. [CrossRef] [PubMed]
65. Marchlinski, F.E.; Callans, D.J.; Gottlieb, C.D.; Zado, E. Linear ablation lesions for control of un-mappable ventricular tachycardia in patients with ischemic and nonischemic cardiomyopathy. *Circulation* **2000**, *101*, 1288. [CrossRef] [PubMed]
66. Wijnmaalen, A.P.; van der Geest, R.J.; van Huls van Taxis, C.F.B.; Siebelink, H.M.J.; Kroft, L.J.M.; Bax, J.J.; Reiber, J.H.; Schalij, M.J.; Zeppenfeld, K. Head-to-head comparison of contrast-enhanced magnetic resonance imaging and electroanatomical voltage mapping to assess post-infarct scar characteristics in patients with ventricular tachycardias: Real-time image integration and reversed registration. *Eur. Heart J.* **2011**, *32*, 104–114. [CrossRef]
67. Vázquez-Calvo, S.; Garre, P.; Sánchez-Somonte, P. Orthogonal high density mapping with VT isthmus analysis vs. pure substrate VT ablation: A case-control study. *Front. Cardiovasc. Med.* **2022**, *9*, 912335. [CrossRef]

68. Yamashita, S.; Sacher, F.; Mahida, S.; Berte, B.; Lim, H.S.; Komatsu, Y.; Amraoui, S.; Denis, A.; Derval, N.; Laurent, F.; et al. Role of high-resolution image integration to visualize left phrenic nerve and coronary arteries during epicardial ventricular tachycardia ablation. *Circ. Arrhythm. Electrophysiol.* **2015**, *8*, 371–380. [CrossRef]
69. Linhart, M.; Alarcon, F.; Borras, R. Delayed gadolinium enhancement magnetic resonance imaging detected anatomic gap length in wide circumferential pulmonary vein ablation lesions is associated with recurrence of atrial fibrillation. *Circ. Arrhythm. Electrophysiol.* **2018**, *11*, e006659. [CrossRef]
70. Chelu, M.G.; King, J.B.; Kholmovski, E.G.; Ma, J.; Gal, P.; Marashly, Q.; AlJuaid, M.A.; Kaur, G.; Silver, M.A.; Johnson, K.A.; et al. Atrial fibrosis by late gadolinium enhancement magnetic resonance imaging and catheter ablation of atrial fibrillation: 5-year follow-up data. *J. Am. Heart Assoc.* **2018**, *7*, e006313. [CrossRef]
71. Khurram, I.M.; Habibi, M.; Gucuk Ipek, E.; Chrispin, J.; Yang, E.; Fukumoto, K.; Dewire, J.; Spragg, D.D.; Marine, J.E.; Berger, R.D.; et al. Left atrial LGE and arrhythmia recurrence following pulmonary vein isolation for paroxysmal and persistent AF. *JACC Cardiovasc. Imaging* **2016**, *9*, 142–148. [CrossRef]
72. Marrouche, N.F.; Wilber, D.; Hindricks, G.; Jais, P.; Akoum, N.; Marchlinski, F.; Kholmovski, E.; Burgon, N.; Hu, N.; Mont, L.; et al. Association of atrial tissue fibrosis identified by delayed enhancement MRI and atrial fibrillation catheter ablation: The DECAAF study. *JAMA* **2014**, *311*, 498–506. [CrossRef]
73. Marrouche, N.F.; Wazni, O.; McGann, C.; Greene, T.; Dean, J.M.; Dagher, L.; Kholmovski, E.; Mansour, M.; Marchlinski, F.; Wilber, D.; et al. Effect of MRI-Guided Fibrosis Ablation vs Conventional Catheter Ablation on Atrial Arrhythmia Recurrence in Patients with Persistent Atrial Fibrillation: The DECAAF II Randomized Clinical Trial. *JAMA* **2022**, *327*, 2296–2305. [CrossRef]
74. Bisbal, F.; Benito, E.; Teis, A.; Alarcón, F.; Sarrias, A.; Caixal, G.; Villuendas, R.; Garre, P.; Soto, N.; Cozzari, J.; et al. Magnetic Resonance Imaging-Guided Fibrosis Ablation for the Treatment of Atrial Fibrillation: The ALICIA Trial. *Circ. Arrhythm. Electrophysiol.* **2020**, *13*, e008707. [CrossRef]
75. Badger, T.J.; Daccarett, M.; Akoum, N.W. Evaluation of left atrial lesions after initial and repeat atrial fibrillation ablation: Lessons learned from delayed-enhancement MRI in repeat ablation procedures. *Circ. Arrhythm. Electrophysiol.* **2010**, *3*, 249–259. [CrossRef]
76. Chubb, H.; Aziz, S.; Karim, R. Optimization of late gadolinium enhancement cardiovascular magnetic resonance imaging of post-ablation atrial scar: A cross-over study. *J. Cardiovasc. Magn. Reson.* **2018**, *20*, 30. [CrossRef]
77. Desjardins, B.; Crawford, T.; Good, E.; Oral, H.; Chugh, A.; Pelosi, F.; Morady, F.; Bogun, F. Infarct architecture and characteristics on delayed enhanced magnetic resonance imaging and electroanatomic mapping in patients with postinfarction ventricular arrhythmia. *Heart Rhythm* **2009**, *6*, 644–651. [CrossRef]
78. Piers, S.R.D.; Tao, Q.; De Riva Silva, M.; Siebelink, H.M.; Schalij, M.J.; Van Der Geest, R.J.; Zeppenfeld, K. CMR-based identification of critical isthmus sites of ischemic and nonischemic ventricular tachycardia. *JACC Cardiovasc. Imaging* **2014**, *7*, 774–784. [CrossRef]
79. Andreu, D.; Ortiz-Perez, J.T.; Boussy, T.; Fernandez-Armenta, J.; Caralt, T.M.; Perea, R.J. Usefulness of contrast-enhanced cardiac magnetic resonance in identifying the ventricular arrhythmia substrate and the approach needed for ablation. *Eur. Heart. J.* **2014**, *35*, 1316–1326. [CrossRef]
80. Acosta, J.; Fernández-Armenta, J.; Penela, D.; Andreu, D.; Borras, R.; Vassanelli, F.; Korshunov, V.; Perea, R.J.; de Caralt, T.M.; Ortiz, J.T.; et al. Infarct transmurality as a criterion for first-line endo-epicardial substrate-guided ventricular tachycardia ablation in ischemic cardiomyopathy. *Heart Rhythm* **2016**, *13*, 85–95. [CrossRef]
81. Quinto, L.; Sanchez, P.; Alarco, F.; Garre, P.; Zaraket, F.; Prat-gonzalez, S. Cardiac magnetic resonance to predict recurrences after ventricular tachycardia ablation: Septal involvement, transmural channels, and left ventricular mass. *Europace* **2021**, *23*, 1437–1445. [CrossRef]
82. Ávila, P.; Pérez-David, E.; Izquierdo, M.; Rojas-González, A.; Sánchez-Gómez, J.M.; Ledesma-Carbayo, M.J. Scar extension measured by magnetic resonancebased nal intensity mapping predicts ventricular tachycardia recurrence after substrate ablation in patients with previous myocardial infarction. *JACC Clin. Electrophysiol.* **2015**, *1*, 353–365. [CrossRef]
83. Nishimura, T.; Patel, H.N.; Wang, S.; Upadhyay, G.A.; Smith, H.L.; Ozcan, C. Prognostic value of cardiac magnetic resonance septal late gadolinium enhancement patterns for periaortic ventricular tachycardia ablation: Heterogeneity of the anteroseptal substrate in nonischemic cardiomyopathy. *Heart Rhythm* **2021**, *18*, 579–588. [CrossRef] [PubMed]
84. Ghafoori, E.; Kholmovski, E.; Thomas, S.; Silvernagel, J.; Nathan, A.; Nan, H. Characterization of gadolinium contrast enhancement of radiofrequency ablation lesions in predicting edema and chronic lesion size. *Circ. Arrhythm. Electrophysiol.* **2017**, *10*, e005599. [CrossRef] [PubMed]
85. Dabbagh, G.S.; Ghannam, M.; Siontis, K.C.; Attili, A.; Cochet, H.; Jais, P.; Eng, M.J.; Latchamsetty, R.; Jongnarangsin, K.; Morady, F.; et al. Magnetic resonance mapping of cathter ablation lesions after postinfarction ventricular tachycardia ablation. *JACC Cardiovasc. Imaging* **2021**, *14*, 588–598. [CrossRef]

Disclaimer/Publisher's Note: The statements, opinions and data contained in all publications are solely those of the individual author(s) and contributor(s) and not of MDPI and/or the editor(s). MDPI and/or the editor(s) disclaim responsibility for any injury to people or property resulting from any ideas, methods, instructions or products referred to in the content.